Polarization properties of low energy amplitude for the $\pi N \to \pi\pi N$ reaction

A. A. Bolokhov, V. A. Kozhevnikov, and D. N. Tatarkin
Sankt-Petersburg State University, Sankt-Petersburg, 198904, Russia

S. G. Sherman
St. Petersburg Institute for Nuclear Physics, Sankt-Petersburg, 188350, Russia

(Received 26 May 1998; revised manuscript received 11 November 1999; published 6 April 2000)

The theoretical study of cross sections for polarized-target measurements of $\pi N \to \pi\pi N$ reactions gives evidence that the interplay between the strong contribution from the one-pion exchange (OPE) mechanism and the one from isobar exchanges, which is equally strong within the isobar half-width energy region, must result in nontrivial polarization phenomena. The Monte Carlo simulations for asymmetries in the $\pi^- p^\uparrow \to \pi^- \pi^+ n$ reaction at $P_{\rm lab}=360$ MeV/c with the use of theoretical amplitudes found as solutions for unpolarized data at $P_{\rm lab}<500$ MeV/c provide confirmations for a significant effect. The effect is capable of discriminating between the OPE and isobar exchanges and it is sensitive to the OPE parameters in question. This leads to the conclusion that the decisive $\pi N \to \pi\pi N$ analysis, aiming at a determination of $\pi\pi$-scattering lengths, must combine both unpolarized data and polarization information. The appropriate measurements are shown to be feasible at the already existing CHAOS spectrometer.

PACS number(s): 13.75.Gx, 13.75.Lb

I. INTRODUCTION

The $\pi N \to \pi\pi N$ reaction is considered to be an essential source of information on $\pi\pi$ scattering. The values of $\pi\pi$-scattering lengths can give restrictions to values of the effective low-energy parameters of QCD obtained within the framework of chiral perturbation theory (ChPT), which was formulated by Gasser and Leutwiller in [1,2] following Weinberg's ideas [3–5]. The appearance of the generalized ChPT (GChPT) scheme [6] enhanced interest in the $\pi\pi$ interaction because of the difference in the predicted $\pi\pi$-scattering lengths with that given by ChPT.

A review of the experimental opportunities for obtaining information on the $\pi\pi$ interaction and a discussion of the status of modern experiments planned to test the ChPT predictions might be found in the talks by Počanić [7,8]. The investigations of $\pi N \to \pi\pi N$ reactions are pronounced to be capable of discriminating between the ChPT and GChPT models for low-energy manifestations of QCD. Meanwhile the most recent attempts [9–13] of an analysis of the $\pi N \to \pi\pi N$ data did not provide the necessary accuracy.

Recently we made an attempt to treat a large set of near-threshold data on total cross sections and one-dimensional (1D) distributions in the energy region $300 \leqslant P_{\rm lab} \leqslant 500$ MeV/c [9]. The phenomenological amplitude for the reaction $\pi N \to \pi\pi N$, taking into account the exchanges of Δ and $N^{(*)}$ along with the one-pion exchange (OPE) mechanism and polynomial background derived with the account of isotopic, crossing, C, P, and T symmetries of strong interactions, was fitted to the experimental data. When calculating our amplitude we use the Feynman graphs with the vertexes written in accordance with chiral theory. Of course we used only tree graphs. The polynomial background stands for the far resonances. The appearance of isobar poles in the physical region of the reaction and, in particular, at the very threshold forces one to extend the standard chiral Lagrangian of the pion-nucleon system by including isobars explicitly. This eliminates the principal advantages of strict theoretical calculations over phenomenologically based ones since plenty of new interaction constants unrestricted by chiral dynamics appears to be taken into account. The phenomenological amplitude can be constructed with account of all symmetries of strong interactions. Hence, the only weakness of the discussed approach is related to minor control of the amplitude's imaginary part as compared to calculations in subsequent orders of ChPT. Indeed, an exact construction of the imaginary part requires information on the phenomenologically unknown process $\pi\pi N \to \pi\pi N$. Nevertheless, the results of an analysis [14] show that isobar resonances saturate the existing data on total cross sections below 1 GeV, so corrections to the imaginary part beyond that given by the Breit-Wigner form of resonance contributions seem to be negligible. Nevertheless, we included the imaginary background in the amplitude.

Though the parameters of OPE are found to be statistically significant, the $\pi\pi$-scattering lengths appear different in different solutions. The origin of the difficulties is attributed to the influence of isobars. Eight parameters of $\pi\pi N\Delta$ and $\pi\pi NN^{(*)}$ interactions, being only weakly constrained by the widths of decays $\Delta \to \pi\pi N$, $N^{(*)} \to \pi\pi N$, strongly correlate with the OPE parameters in question.

The essential difficulty originates from limitations to data of unpolarized measurements which cannot discriminate between contributions to different spin structures of the reaction amplitude. Up to now the known polarization measurements of the $\pi N \to \pi\pi N$ reactions have been performed at considerably higher energies, for example, at 5.98 GeV/c and 11.85 GeV/c [15] and at 17.2 GeV/c [16]. The analyses of the polarized data [17,18] already proved such measurements to be detailed sources of information on the $\pi\pi$ interaction.

The main goals of the present paper are to elaborate the theoretical framework for treating the polarization measurements of $\pi N \to \pi\pi N$ reactions at low energies and to find out the suitable observables. We pay separate attention to a study of the principal possibility to perform polarized πN

 ©2000 The American Physical Society

$\rightarrow \pi\pi N$ experiments at the already existing CHAOS spectrometer [19]. The primary goal is to ensure the solution of an urgent problem: the obtaining of the $\pi\pi$-scattering characteristics with the help of the solid bank of available $\pi N \rightarrow \pi\pi N$ data and simple polarization measurements added.

We base our analysis upon the general properties of the $\pi N \rightarrow \pi\pi N$ amplitude. It describes five charge channels in terms of only four isoscalar functions. Moreover, three of these functions are strongly restricted by crossing symmetry to only one independent function (see [20–22]). To take advantage of the intimate relations between various channels we prefer to rely upon the crossing symmetry rather than the partial-wave expansion.

The paper is organized as follows. The content of Sec. II reviews the structure of the $\pi N \rightarrow \pi\pi N$ amplitude. Section III provides expressions necessary for calculations of cross sections in experiments with a polarized target. Section IV is devoted to the geometry of devices and analyzed asymmetries. It contains the results of modeling the experimental measurements with the use of various solutions found in Ref. [9] for the $\pi N \rightarrow \pi\pi N$ amplitude. The summary, the concluding remarks, and a discussion of implementations are given in Sec. V.

II. GENERAL STRUCTURE OF THE $\pi N \rightarrow \pi\pi N$ AMPLITUDE

This short section introduces the basic formulas of Refs. [22,9].

We consider the reaction

$$\pi^a(k_1)+N_\alpha(p;\lambda_i)\rightarrow\pi^b(k_2)+\pi^c(k_3)+N_\beta(q;\lambda_f), \quad (1)$$

where $a,b,c=1,2,3$ and $\alpha,\beta=1,2$ are isotopic indices of pions and nucleons, respectively, and λ_i (λ_f) are polarizations of initial (final) nucleons.

Separating the nucleon spinor wave functions from the reaction amplitude $M^{abc}_{\beta\alpha}(\lambda_f;\lambda_i)$,

$$M^{abc}_{\beta\alpha}(\lambda_f;\lambda_i)=\overline{u}(q;\lambda_f)\hat{M}^{abc}_{\beta\alpha}(i\gamma_5)u(p;\lambda_i), \quad (2)$$

one can define the isoscalar amplitudes $\hat{A}$, $\hat{B}$, $\hat{C}$, $\hat{D}$ by

$$\hat{M}^{abc}_{\beta\alpha}=\hat{A}\tau^a_{\beta\alpha}\delta^{bc}+\hat{B}\tau^b_{\beta\alpha}\delta^{ac}+\hat{C}\tau^c_{\beta\alpha}\delta^{ab}+\hat{D}i\epsilon^{abc}\delta_{\beta\alpha}, \quad (3)$$

τ^a, $a=1,2,3$, being the nucleon-isospin generators. The amplitudes of five observable channels are related to A,B,C,D by

$$\begin{aligned}
\hat{M}_{\{\pi^-p\rightarrow\pi^-\pi^+n\}}&=\sqrt{2}/2(\hat{A}+\hat{C}),\\
\hat{M}_{\{\pi^-p\rightarrow\pi^0\pi^0n\}}&=1/2(\hat{A}),\\
\hat{M}_{\{\pi^-p\rightarrow\pi^-\pi^0p\}}&=1/2(\hat{C}-2\hat{D}),\\
\hat{M}_{\{\pi^+p\rightarrow\pi^+\pi^0p\}}&=1/2(\hat{C}+2\hat{D}),\\
\hat{M}_{\{\pi^+p\rightarrow\pi^+\pi^+n\}}&=1/2(\hat{B}+\hat{C}).
\end{aligned} \quad (4)$$

To simplify the processing of cross sections, the statistical factors accounting for identical pions are inserted into these definitions. Below, we leave only the charges of the final pions as subscripts for the channels.

To decompose each isoscalar function $\hat{A},\hat{B},\hat{C},\hat{D}$ and each amplitude $\hat{M}_X$, $X=\{-+n\}$, $\{-0p\}$, $\{00n\}$, $\{++n\}$, $\{+0p\}$, into independent spinor form factors let us define the crossing-covariant complex combinations $k=k_R+ik_I$, $\overline{k}=k_R-ik_I$ of pion momenta:

$$k=-k_1+\epsilon k_2+\overline{\epsilon}k_3, \quad \overline{k}=-k_1+\overline{\epsilon}k_2+\epsilon k_3, \quad (5)$$

$$k_R=-k_1-(k_2+k_3)/2, \qquad k_I=\sqrt{3}(k_2-k_3)/2, \quad (6)$$

where $\epsilon\equiv\exp(2\pi i/3)=-1/2+i\sqrt{3}/2$, $\overline{\epsilon}=\epsilon^*=-1/2-i\sqrt{3}/2$. The decomposition reads

$$\begin{aligned}
\hat{M}_X&=S_X+\overline{V}_X\hat{k}+V_X\hat{\overline{k}}+i/2T_X[\hat{k},\hat{\overline{k}}]\\
&\equiv\begin{pmatrix}S_X\\ \overline{V}_X\\ V_X\\ T_X\end{pmatrix}^{\mathrm{T}}\cdot\begin{pmatrix}\hat{1}\\ \hat{k}\\ \hat{\overline{k}}\\ i/2[\hat{k},\hat{\overline{k}}]\end{pmatrix}\\
&(X=\{-+n\},\{-0p\},\{00n\},\{++n\},\{+0p\}).
\end{aligned} \quad (7)$$

Since polarization phenomena are determined by the interference of real and imaginary parts of the amplitude, it is convenient to deal with the combinations

$$S_X, \quad V_X^R\equiv(V_X+\overline{V}_X)/2, \quad V_X^I\equiv(V_X-\overline{V}_X)/(2i), \quad T_X, \quad (8)$$

which are shown to be approximately real in the energy region where unitarity corrections are small (see [21]). So we rewrite the decomposition (7) in the form

$$\begin{aligned}
\hat{M}_X&=\begin{pmatrix}S_X\\ V_X^R\\ V_X^I\\ T_X\end{pmatrix}^{\mathrm{T}}\cdot\begin{pmatrix}\hat{1}\\ 2\hat{k}_R\\ 2\hat{k}_I\\ [\hat{k}_R,\hat{k}_I]\end{pmatrix}\\
&(X=\{-+n\},\{-0p\},\{00n\},\{++n\},\{+0p\}).
\end{aligned} \quad (9)$$

The matrix element $||M||^2$ entering the unpolarized cross section is the sum over final polarizations and the average over initial ones. It is the quadratic form of the vector of spinor form factors (S_X,V_X^R,V_X^I,T_X):

$$\|M_X\|^2 \equiv 1/2 \sum_{\lambda_f,\lambda_i} [\overline{u}(q;\lambda_f)\hat{M}_X(i\gamma_5)u(p;\lambda_i)] \times [\overline{u}(q;\lambda_f)\hat{M}_X(i\gamma_5)u(p;\lambda_i)]^* = \begin{pmatrix} S_X \\ V_X^R \\ V_X^I \\ T_X \end{pmatrix}^{\mathrm{T}} G_R \begin{pmatrix} S_X \\ V_X^R \\ V_X^I \\ T_X \end{pmatrix}^* = \begin{pmatrix} S_X \\ V_X^R \\ V_X^I \\ T_X \end{pmatrix}^{\dagger} G_R \begin{pmatrix} S_X \\ V_X^R \\ V_X^I \\ T_X \end{pmatrix} \quad (10)$$

$$(X=\{--n\},\{-0p\},\{00n\},\{++n\},\{+0p\}).$$

The real Hermitian matrix G_R is obtained by calculating the γ-matrix traces

$$G_R \equiv \frac{1}{2}\mathrm{Sp}\left[(\hat{q}+m) \begin{Bmatrix} \hat{1} \\ 2\hat{k}_R \\ 2\hat{k}_I \\ [\hat{k}_R,\hat{k}_I] \end{Bmatrix} (\hat{p}-m)\gamma_0 \begin{Bmatrix} \hat{1} \\ 2\hat{k}_R \\ 2\hat{k}_I \\ [\hat{k}_R,\hat{k}_I] \end{Bmatrix}^{\dagger} \gamma_0 \right]. \quad (11)$$

Its explicit expression will be given below; see Eqs. (14).

III. CROSS SECTION FOR POLARIZED-TARGET MEASUREMENTS

The origin of the strong correlations between parameters of the OPE and isobar contributions, preventing an accurate determination of the $\pi\pi$-scattering lengths in the unpolarized experiment, is obvious now. Only the specific combination of the competing contributions given by Eq. (10) can be measured in such experiments. Bringing this matrix to diagonal form one can realize that any diagonal amplitude can mimic the OPE one outside the region of isobar poles.

Though measurement of the final polarization in the $\pi N \to \pi\pi N$ reaction is implied by the design of the spectrometer AMPIR (see [23]), such measurements are hardly to be performed in the near future. Therefore, we consider the polarized-target experimental setup. For simplicity, we assume an ideal polarization. It is easy to generalize our results to the incomplete polarization due to the linear dependence of all asymmetries upon the polarization vector **s**. Indeed, given the nontrivial probabilities w_{λ_1}, w_{λ_2} $(w_{\lambda_1}+w_{\lambda_2}=1)$ for the projection of the initial nucleon spin in the direction $\mathbf{n_s}\equiv\mathbf{s}/|\mathbf{s}|$ to be $\lambda_1=1/2$, $\lambda_2=-1/2$, respectively, any theoretical result for asymmetry must be derived with $|\mathbf{s}|=w_{\mathbf{s}}=2w_{\lambda_1}-1=w_{\lambda_1}-w_{\lambda_2}$. We set $w_{\mathbf{s}}=1$ in calculations.

The matrix element $\|M\|_{\mathbf{s}}^2$ is now defined by

$$\|M_X\|_{\mathbf{s}}^2 \equiv \sum_{\lambda_f} [\overline{u}(q;\lambda_f)\hat{M}_X(i\gamma_5)u(p;\lambda_i)] \times [\overline{u}(q;\lambda_f)\hat{M}_X(i\gamma_5)u(p;\lambda_i)]^* = \begin{pmatrix} S_X \\ V_X^R \\ V_X^I \\ T_X \end{pmatrix}^{\mathrm{T}} G \begin{pmatrix} S_X \\ V_X^R \\ V_X^I \\ T_X \end{pmatrix}^* = \begin{pmatrix} S_X \\ V_X^R \\ V_X^I \\ T_X \end{pmatrix}^{\dagger} G^* \begin{pmatrix} S_X \\ V_X^R \\ V_X^I \\ T_X \end{pmatrix} \quad (12)$$

$$(X=\{--n\},\{-0p\},\{00n\},\{++n\},\{+0p\}).$$

The Hermitian matrix $G\equiv G_R+iG_I$ is given by

$$G \equiv \mathrm{Sp}\left[(\hat{q}+m_f) \begin{Bmatrix} \hat{1} \\ 2\hat{k}_R \\ 2\hat{k}_I \\ [\hat{k}_R,\hat{k}_I] \end{Bmatrix} \times (\hat{p}-m_i)\frac{1+\gamma_5\hat{s}}{2}\gamma_0 \begin{Bmatrix} \hat{1} \\ 2\hat{k}_R \\ 2\hat{k}_I \\ [\hat{k}_R,\hat{k}_I] \end{Bmatrix}^{\dagger} \gamma_0 \right], \quad (13)$$

where the polarization four-vector s equals $(0,\mathbf{s})$ in the rest frame of the initial nucleon.

The real part G_R of this matrix enters the unpolarized cross section [cf. Eqs. (11) and (13)]. The imaginary part G_I is skew symmetric. These matrices are explicitly given by

$$\begin{aligned}
G_R(1,1) &= 2(-m_i m_f + p\cdot q),\\
G_R(1,2) &= 4(-m_i q\cdot k_R + m_f p\cdot k_R),\\
G_R(1,3) &= 4(-m_i q\cdot k_I + m_f p\cdot k_I),\\
G_R(1,4) &= 4(-p\cdot k_R q\cdot k_I + q\cdot k_R p\cdot k_I),\\
G_R(2,2) &= 8(-m_i m_f k_R\cdot k_R - p\cdot q k_R\cdot k_R + 2p\cdot k_R q\cdot k_R),\\
G_R(2,3) &= 8(-m_i m_f k_R\cdot k_I - p\cdot q k_R\cdot k_I + p\cdot k_R q\cdot k_I + q\cdot k_R p\cdot k_I),\\
G_R(2,4) &= 8(-m_i q\cdot k_R k_R\cdot k_I + m_i q\cdot k_I k_R\cdot k_R - m_f p\cdot k_R k_R\cdot k_I + m_f p\cdot k_I k_R\cdot k_R),\\
G_R(3,3) &= 8(-m_i m_f k_I\cdot k_I - p\cdot q k_I\cdot k_I + 2p\cdot k_I q\cdot k_I),\\
G_R(3,4) &= 8(-m_i q\cdot k_R k_I\cdot k_I + m_i q\cdot k_I k_R\cdot k_I - m_f p\cdot k_R k_I\cdot k_I + m_f p\cdot k_I k_R\cdot k_I),\\
G_R(4,4) &= 8(-m_i m_f k_R\cdot k_R k_I\cdot k_I + m_i m_f (k_R\cdot k_I)^2 + p\cdot q k_R\cdot k_R k_I\cdot k_I - p\cdot q (k_R\cdot k_I)^2 - 2p\cdot k_R q\cdot k_R k_I\cdot k_I + 2p\cdot k_R q\cdot k_I k_R\cdot k_I + 2q\cdot k_R p\cdot k_I k_R\cdot k_I - 2p\cdot k_I q\cdot k_I k_R\cdot k_R),
\end{aligned} \quad (14)$$

$$\begin{aligned}
G_I(1,2) &= -4\ \mathrm{eps}[p,q,s,k_R],\\
G_I(1,3) &= -4\ \mathrm{eps}[p,q,s,k_I],\\
G_I(1,4) &= 4\,(\mathrm{eps}[p,s,k_R,k_I]m_f - \mathrm{eps}[q,s,k_R,k_I]m_i),
\end{aligned}$$

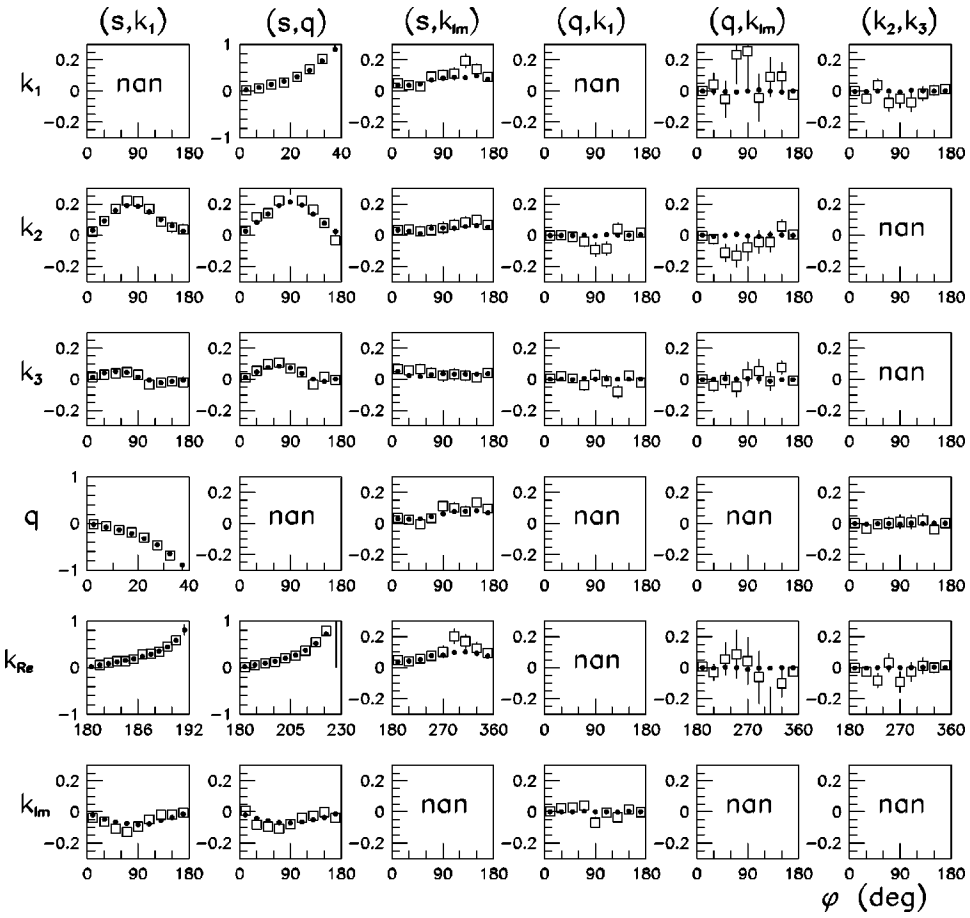

FIG. 1. Asymmetries for the amplitude solw6 at $(\mathbf{s}\perp\mathbf{k}_1)$ in the 4π-steradian geometry device (solid circles) and in CHAOS (open squares); $\pi^- p^\uparrow \to \pi^- \pi^+ n$ reaction at $P_{\rm Lab}=360$ MeV/c. In the heads of the column in parentheses are printed two vectors describing the asymmetry plane. The abbreviation ''nan'' denotes that the vector printed on left of the row cannot have asymmetry regarding this plane.

$$
\begin{aligned}
G_I(2,3) &= 8\,(\mathrm{eps}[p,s,k_R,k_I]m_f + \mathrm{eps}[q,s,k_R,k_I]m_i),\\
G_I(2,4) &= 8\,(\mathrm{eps}[p,q,s,k_R]k_R\cdot k_I - \mathrm{eps}[p,q,s,k_I]k_R\cdot k_R\\
&\quad + 2\,\mathrm{eps}[p,q,k_R,k_I]s\cdot k_R\\
&\quad + 2\,\mathrm{eps}[q,s,k_R,k_I]p\cdot k_R),\\
G_I(3,4) &= 8\,(\mathrm{eps}[p,q,s,k_R]k_I\cdot k_I - \mathrm{eps}[p,q,s,k_I]k_R\cdot k_I\\
&\quad + 2\,\mathrm{eps}[p,q,k_R,k_I]s\cdot k_I + 2\,\mathrm{eps}[q,s,k_R,k_I]p\cdot k_I),
\end{aligned}
\tag{15}
$$

where the notation

$$
\mathrm{eps}[x,y,u,v] \equiv \epsilon_{\mu\nu\rho\sigma}x^\mu y^\nu u^\rho v^\sigma
$$

is used and the nucleon masses m_i, m_f are allowed to be different. The matrix elements in Eqs. (15) are actually ordered according to their importance in the near-threshold region.

Let us now consider the fixed reaction channel and omit the channel's subscript in the notation for the vector M of form factors (8). The form factors V^R, V^I are obtained by splitting off the real and imaginary parts in the cross-covariant momenta of the spinor structures $\hat{k}$, $\widehat{k}$. The form factors themselves remain complex: $V^R \equiv V_R^R + iV_I^R$, $V^I \equiv V_R^I + iV_I^I$. Consider the real and imaginary parts of the amplitude:

$$
M_R \equiv \begin{pmatrix} S_R \\ V_R^R \\ V_R^I \\ T_R \end{pmatrix}, \quad M_I \equiv \begin{pmatrix} S_I \\ V_I^R \\ V_I^I \\ T_I \end{pmatrix}. \tag{16}
$$

Then the matrix element (12) can be rewritten as

$$
\|M\|_{\mathbf{s}}^2 = M_R^{\mathrm{T}} G_R M_R + M_I^{\mathrm{T}} G_R M_I + 2 M_R^{\mathrm{T}} G_I M_I . \tag{17}
$$

Here, the first two terms on the right-hand side give the unpolarized matrix element (10). The effect of polarization is provided by the third term.

Two conclusions can be immediately derived from this form and the above explicit expressions for matrices G_R, G_I.

(i) OPE contributes only to the spinor form factor S of the decompositions (7), (9). Hence, the validity of the assumption about OPE dominance means that there cannot be any asymmetry in the reaction cross sections at the energies where the assumption holds.

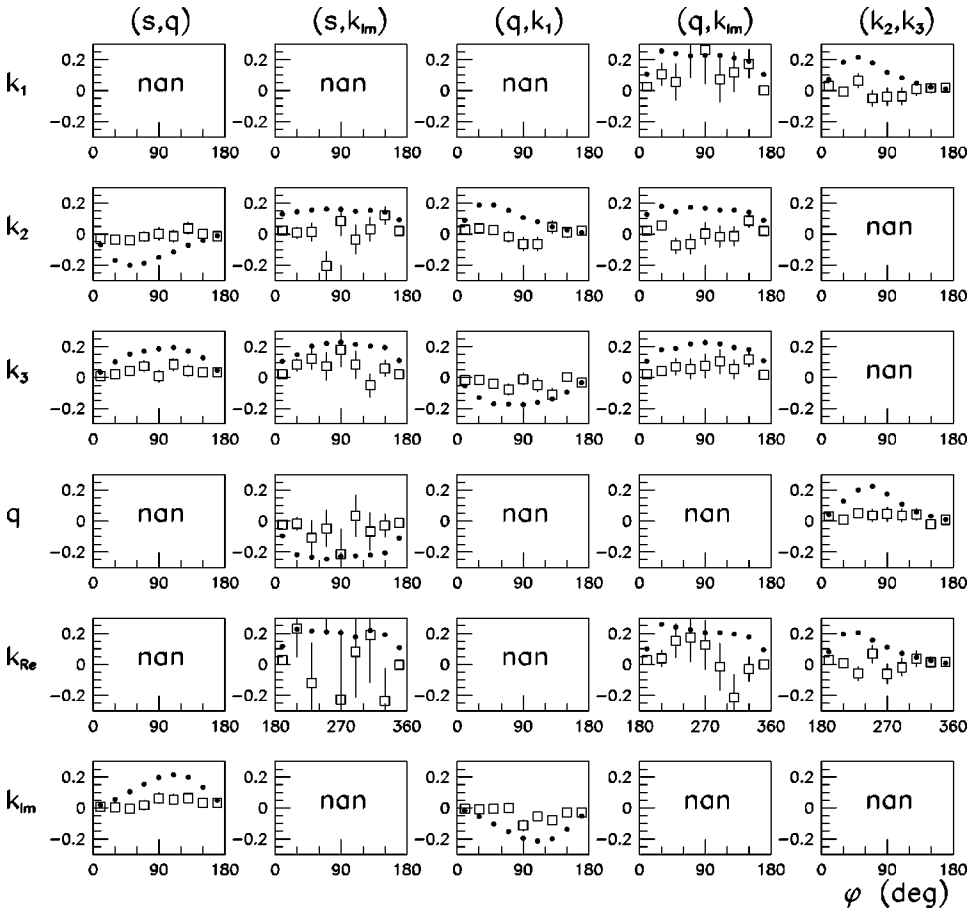

FIG. 2. Asymmetries for the amplitude solw6 at $(\mathbf{s}||\mathbf{k}_1)$ in the 4π-steradian geometry device (solid circles) and in CHAOS (open squares); $\pi^- p^\uparrow \to \pi^- \pi^+ n$ reaction at $P_{\rm lab}=360$ MeV/c.

(ii) It is necessary for the polarization effect that both the real and imaginary parts of the amplitude remain non-negligible. Fortunately, several partial waves are mixed up in the polarization term of Eq. (17). So the polarization effect must manifest itself in asymmetries of cross sections not only at the isobar poles ($P_{\rm lab}\approx 500$ Mev/c for Δ and $P_{\rm lab}\approx 660$ Mev/c for $N^{(*)}$) but well below due to the large widths of these resonances.

We included the polynomial background to the imaginary part of the amplitude in the same manner as in the real part. The parameters of the real and imaginary backgrounds are independent and are determined in the course of experimental data fitting. The parameters are bound by the condition that the amplitude phases at the reaction threshold be equal to P-wave phases of the elastic πN amplitude [24]. So the imaginary part of our amplitude is not determined entirely by the widths of the resonances.

The rich kinematics of the considered reaction gives rise to an abundance of possibilities for the manifestation of polarization in the polarized-target experiments. There are five distinct structures entering the matrix G_I of Eq. (17). These are

$$\mathrm{eps}[p,q,s,k_R] = -3/2\,\mathrm{eps}[p,q,s,k_1], \tag{18}$$

$$\mathrm{eps}[p,q,s,k_I], \tag{19}$$

$$\mathrm{eps}[p,s,k_R,k_I], \tag{20}$$

$$\mathrm{eps}[q,s,k_R,k_I], \tag{21}$$

$$\mathrm{eps}[p,q,k_R,k_I] = -3\sqrt{3}/4\,\mathrm{eps}[p,q,k_1,k_2-k_3]. \tag{22}$$

One finds that, depending on the relative strength of form factors (16), any of the above structures can govern the discussed effects. Four structures (18), (19), (20), and (21), entering matrix elements $G_I(1,2)$, $G_I(1,3)$, and $G_I(1,4)$ related to OPE, are also present in the rest elements given by Eqs. (15). At small $\mathbf{q}$, $\mathbf{k}_2$, and $\mathbf{k}_3$, the terms (18) and (19) are the most favorable ones for detecting OPE since extra factors in the same terms in $G_I(2,3)$, $G_I(2,4)$, and $G_I(3,4)$ eliminate the effect when averaged. At the same time, there is the single term (22) which is specific to non-OPE contributions only. It can be ''switched off'' by a $(s\cdot k_R)$ factor since the vector $\mathbf{k}_R$ belongs to a narrow backward cone at low energies. This phenomenon is a characteristic feature of non-OPE mechanisms.

Let two vectors $\mathbf{x}$ and $\mathbf{y}$ determine the plane $(\mathbf{x},\mathbf{y})$, separating ''left'' and ''right'' semispheres, and $\mathbf{z}$ be some third vector. Let $\varphi_{\mathbf{z}}$ be its azimuthal angle in the plane which contains $\mathbf{y}$ and is orthogonal to the plane $(\mathbf{x},\mathbf{y})$. The asymmetry

TABLE I. The largest asymmetries for $\pi^- p \to \pi^- \pi^+ n$ channel at $P_{\rm lab}=360$ MeV/c. The last-digit errors are given in parentheses.

Ampl.	$a_0^{I=0}$	$a_0^{I=2}$	$a_1^{I=1}$	$(\mathbf{s}\perp\mathbf{k}_1)$ 4π	$(\mathbf{s}\perp\mathbf{k}_1)$ CHAOS	$(\mathbf{s}\|\|\mathbf{k}_1)$ 4π
solw6	0.264	−0.008	0.032	$0.89(4)_{(\mathbf{s},\mathbf{q})}(\mathbf{k}_1)$	$0.91(7)_{(\mathbf{s},\mathbf{q})}(\mathbf{k}_1)$	$0.259(4)_{(\mathbf{q},\mathbf{k}_I)}(\mathbf{k}_R)$
Expt.	0.26	−0.028	0.038	$0.70(4)_{(\mathbf{s},\mathbf{q})}(\mathbf{k}_1)$	$0.72(7)_{(\mathbf{s},\mathbf{q})}(\mathbf{k}_1)$	$0.35(4)_{(\mathbf{q},\mathbf{k}_I)}(\mathbf{k}_R)$
ChPT	0.20	−0.042	0.037	$0.80(4)_{(\mathbf{s},\mathbf{q})}(\mathbf{k}_1)$	$0.80(7)_{(\mathbf{s},\mathbf{q})}(\mathbf{k}_1)$	$0.40(4)_{(\mathbf{q},\mathbf{k}_I)}(\mathbf{k}_R)$
sol06	0.189	−0.059	0.054	$-0.38(4)_{(\mathbf{s},\mathbf{k}_1)}(\mathbf{k}_R)$	$-0.40(6)_{(\mathbf{s},\mathbf{k}_1)}(\mathbf{k}_R)$	$0.089(6)_{(\mathbf{q},\mathbf{k}_I)}(\mathbf{k}_R)$
sol10	0.172	−0.043	0.050	$-0.41(3)_{(\mathbf{s},\mathbf{k}_1)}(\mathbf{q})$	$0.39(4)_{(\mathbf{s},\mathbf{q})}(\mathbf{k}_1)$	$0.133(3)_{(\mathbf{q},\mathbf{k}_I)}(\mathbf{k}_R)$
sol03	0.069	−0.057	0.045	$-0.29(3)_{(\mathbf{s},\mathbf{k}_1)}(\mathbf{q})$	$0.25(4)_{(\mathbf{s},\mathbf{q})}(\mathbf{k}_1)$	$0.265(8)_{(\mathbf{s},\mathbf{k}_I)}(\mathbf{k}_2)$
sol11	0.067	−0.077	0.047	$0.48(3)_{(\mathbf{s},\mathbf{k}_1)}(\mathbf{q})$	$0.52(5)_{(\mathbf{s},\mathbf{k}_1)}(\mathbf{q})$	$0.224(7)_{(\mathbf{q},\mathbf{k}_I)}(\mathbf{k}_R)$

$$A_{(\mathbf{x},\mathbf{y})}(\varphi_{\mathbf{z}}) \equiv \frac{\sigma(\varphi_{\mathbf{z}})-\sigma(-\varphi_{\mathbf{z}})}{\sigma(\varphi_{\mathbf{z}})+\sigma(-\varphi_{\mathbf{z}})} \tag{23}$$

shows the relative value of the polarization term of Eq. (17) with respect to unpolarized cross sections. Obviously, several asymmetries must be observed to detect the influence of all of the above structures (18)–(22).

It was already pointed out in the beginning of this section that the above formulas (12), (13), (14), (15), and (17) remain valid for incomplete polarization of the target, the vector $s \equiv s_i$ being recognized as the polarization vector of the density matrix ρ_i for the initial nucleon. The density matrix for the final nucleon $\rho_f \equiv \frac{1}{2}(\hat{q}+m_f)(1-\gamma_5 \hat{s}_f)$ is given by

$$\rho_f = \frac{(\hat{q}+m_f)\hat{M}(i\gamma 5)\rho_i \gamma_0 (i\gamma 5)^\dagger \hat{M}^\dagger \gamma_0 (\hat{q}+m_f)}{\mathrm{Sp}[(\hat{q}+m_f)\hat{M}(i\gamma 5)\rho_i \gamma_0 (i\gamma 5)^\dagger \hat{M}^\dagger \gamma_0]}. \tag{24}$$

The expression for the polarization vector s_f takes the form

$$s_f^\mu = \frac{1}{2m_f}\frac{M^{\mathrm{T}} F^\mu M^*}{M^{\mathrm{T}} G M^*}, \tag{25}$$

where G is given by Eqs. (13), (14), and (15) and the array of matrices F^μ can be calculated as

$$F^\mu \equiv \mathrm{Sp}\left[(\hat{q}+m_f) \begin{Bmatrix} \hat{1} \\ 2\hat{k}_R \\ 2\hat{k}_I \\ [\hat{k}_R,\hat{k}_I] \end{Bmatrix} \times (\hat{p}-m_i)\frac{1+\gamma_5 \hat{s}_i}{2}\gamma_0 \begin{Bmatrix} \hat{1} \\ 2\hat{k}_R \\ 2\hat{k}_I \\ [\hat{k}_R,\hat{k}_I] \end{Bmatrix}^\dagger \gamma_0 (\hat{q}+m_f)\gamma_5 \gamma^\mu \right]. \tag{26}$$

The calculation with the use of the standard high-energy physics package of computer algebra [25] is straightforward, the result being too cumbersome to be displayed here.

The values of s_f and $A_{(\mathbf{x},\mathbf{y})}(\varphi_{\mathbf{z}})$ are defined over four-dimensional phase space of the considered reaction. This makes it difficult to display such quantities visually. Below, we consider asymmetries which are integrated as over ''orange lobules'' of $\varphi_{\mathbf{z}}$ bins, $\mathbf{z}$ being a selected momentum, as well as over the allowed range of the rest momenta. This averaging suppresses the polarization effect. The suppression depends upon the kinematical symmetry of the considered amplitude: the more symmetry displayed by the amplitude, the less the value of the averaged asymmetry $A_{(\mathbf{x},\mathbf{y})}(\varphi_{\mathbf{z}})$ obtained. It was shown in Ref. [21] that the form factors S, V^R, V^I, and T of isoscalar amplitudes A, B, C, and D had definite properties under permutation of nucleons $p \leftrightarrow -q$ due to charge-conjugation symmetry, the properties of D-amplitude form factors being opposite to the ones of the corresponding form factors of the rest isoscalar amplitudes. Another symmetry of particle momenta, which eliminates kinematical degrees of freedom, is related to Bose statistics of identical

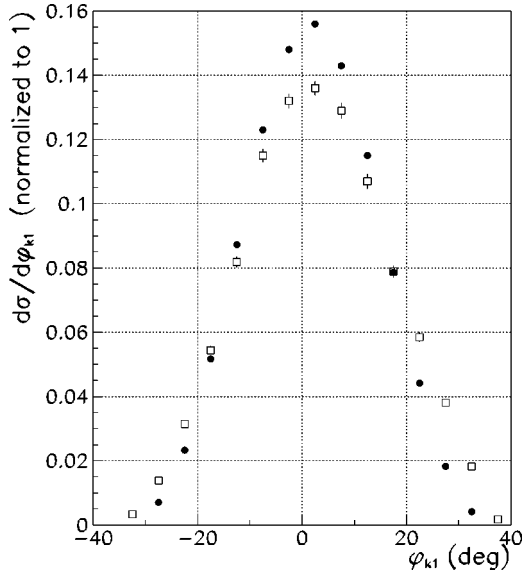

FIG. 3. Normalized theoretical distributions in the azimuth angle of $\mathbf{k}_1$ projected onto the plane through $\mathbf{q}$ and orthogonal to the plane $(\mathbf{s},\mathbf{q})$ for the amplitude solw6 at $(\mathbf{s}\perp\mathbf{k}_1)$ in the 4π-steradian geometry device (solid circles) and in CHAOS (open squares); $\pi^- p^\uparrow \to \pi^- \pi^+ n$ reaction at $P_{\rm lab}=360$ MeV/c.

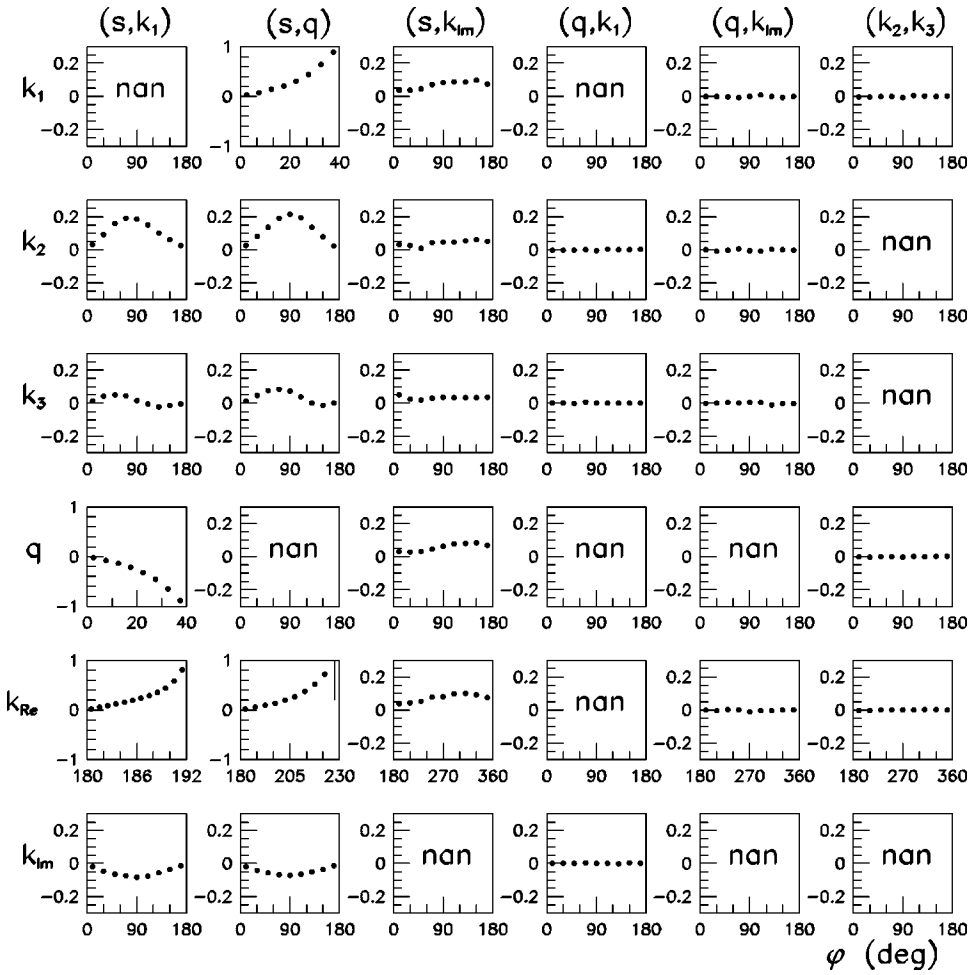

FIG. 4. Asymmetries for the amplitudes sol06 (open circles), sol03 (open squares), sol10 (open triangles), and solw6 (solid circles) at $(\mathbf{s}\perp\mathbf{k}_1)$ in the 4π-steradian geometry device; $\pi^- p^\uparrow \to \pi^-\pi^+ n$ reaction at $P_{\mathrm{Lab}}=360$ MeV/c.

pions in $\{++n\}$ and $\{00n\}$ channels. The expressions for channel amplitudes given by Eqs. (4) show that the asymmetries for the above two channels suffer more from the discussed degeneracy than the asymmetries of the channels $\{\pm 0p\}$. Being free from the degeneracy, these channels can display less suppression under averaging. It is obvious that the rare events in the reaction represent the only reason for considering the integral quantities.

IV. SIMULATION OF DATA AND RESULTS

It is found necessary to study asymmetries of cross sections with respect to various planes in momentum space. The complicated form of the phenomenological amplitude makes it impossible to perform an analytic investigation of the polarization term of the matrix element (17). In the absence of real experimental measurements, we perform theoretical simulations. Prior to a discussion of their details given below, let us briefly consider the geometry of the existing CHAOS device which is capable of providing the necessary measurements (for more details see [19,26,27]).

The cylindrical dipole magnet, producing a vertical magnetic field, is the largest part of the CHAOS spectrometer. A polarized target is exposed to the horizontal pion beam. The target is inserted through the 120 mm caliber hole along the magnet's symmetry axis. So the target is placed at the center of the cylindrical space between the magnet poles, the pole diameter being 950 mm. Four cylindrical chambers are surrounding the target: the most inner WC1 and WC2 are fast multiwire proportional chambers; WC3 and WC4 are the drift chambers.

The ring of gain-stabilized counter telescopes constitutes the outside layer of detectors. These counters determine a vertical acceptance of $\pm 7°$. In the horizontal plane (CHAOS plane), there are deadened regions of WC3 and WC4 at narrow angles ($\approx 36°$ in total) where the beam enters and exits the device. This causes a difficulty for tracking and particle identification for some events. The angle and momentum value of an outgoing charged particle hitting only WC1 and WC2 and missing WC3 and/or WC4 are correlated because of the magnetic field present. We neglect this effect and simply set the horizontal acceptance to 360°. Apart from geometrical cuts, no extra factors such as efficiencies of registration, etc., are involved in our simulations for simplicity.

Though some structures of polarized cross sections, like that of Eqs. (19) and (22), have no explicit dependence upon the relative orientation of the nucleon-spin vector **s** and the beam $\mathbf{k}_1$, we consider two basic variants with respect to this

orientation in the laboratory system. This is natural for the design of experimental devices and this is convenient for data simulations as well. So **s** is chosen to be orthogonal to the beam $\mathbf{k}_1$ and to the CHAOS plane in the first variant ($\mathbf{s}\perp\mathbf{k}_1$) and **s** is chosen to be parallel to the beam $\mathbf{k}_1$ in the second variant ($\mathbf{s}||\mathbf{k}_1$).

The Monte Carlo events for the reaction channel $\pi^- p^\uparrow \to \pi^-\pi^+ n$ are generated at the beam momentum set to $P_{\rm lab}=360$ MeV/c. Few control runs are performed also for the rest channels at the same energy. We consider the azimuth angle in the plane orthogonal to ($\mathbf{x},\mathbf{y}$) through the vector **y**. The angle is counted out from the direction **y**. The bins for this angle are filled with the selection of events (a) without geometrical restrictions and (b) with restrictions of CHAOS geometry (CHAOS is hit by 46 307 events from the requested amount of 2 000 000).

A list of examined asymmetries $A_{(\mathbf{x},\mathbf{y})}(\varphi_{\mathbf{z}})$ can be obtained from the headings of Figs. 1 and 2. For obvious geometrical reasons the list for the variant ($\mathbf{s}||\mathbf{k}_1$) is truncated. The list is far from being complete combinatorically. Nevertheless, it is sufficient to display the role of distinct structures and to demonstrate the tight relations between quantities like $A_{(\mathbf{s},\mathbf{k}_1)}(\varphi_{\mathbf{q}})$ and $A_{(\mathbf{s},\mathbf{q})}(\varphi_{\mathbf{k}_1})$.

TABLE II. Modern three sets of $\pi\pi$ amplitude parameters.

	Expt.	ChPT	GChPT
$a_0^{I=0}$	0.26	0.20	0.263
$b_0^{I=0}$	0.25	0.25	0.25
$a_0^{I=2}$	−0.028	−0.042	−0.027
$b_0^{I=2}$	−0.082	−0.073	−0.079
$a_1^{I=1}$	0.038	0.037	0.037
$b_1^{I=1}$		0.0048	0.0054
$a_2^{I=2}$	0.0017	0.0018	
$b_2^{I=2}$	0.00013	0.00021	

The building of the phenomenological $\pi N\to\pi\pi N$ amplitude is an approach which in principle allows one to determine the parameters of the $\pi\pi$ amplitude. But it turned out to be impossible to perform it without polarization observables. The serious difficulty was the appearance of a lot of solutions with nonphysical values of $\pi\pi$-scattering lengths. We would like to demonstrate now which measurement of asymmetry can resolve this problem to some extent.

Many amplitudes for $\pi N\to\pi\pi N$ reactions, all of which

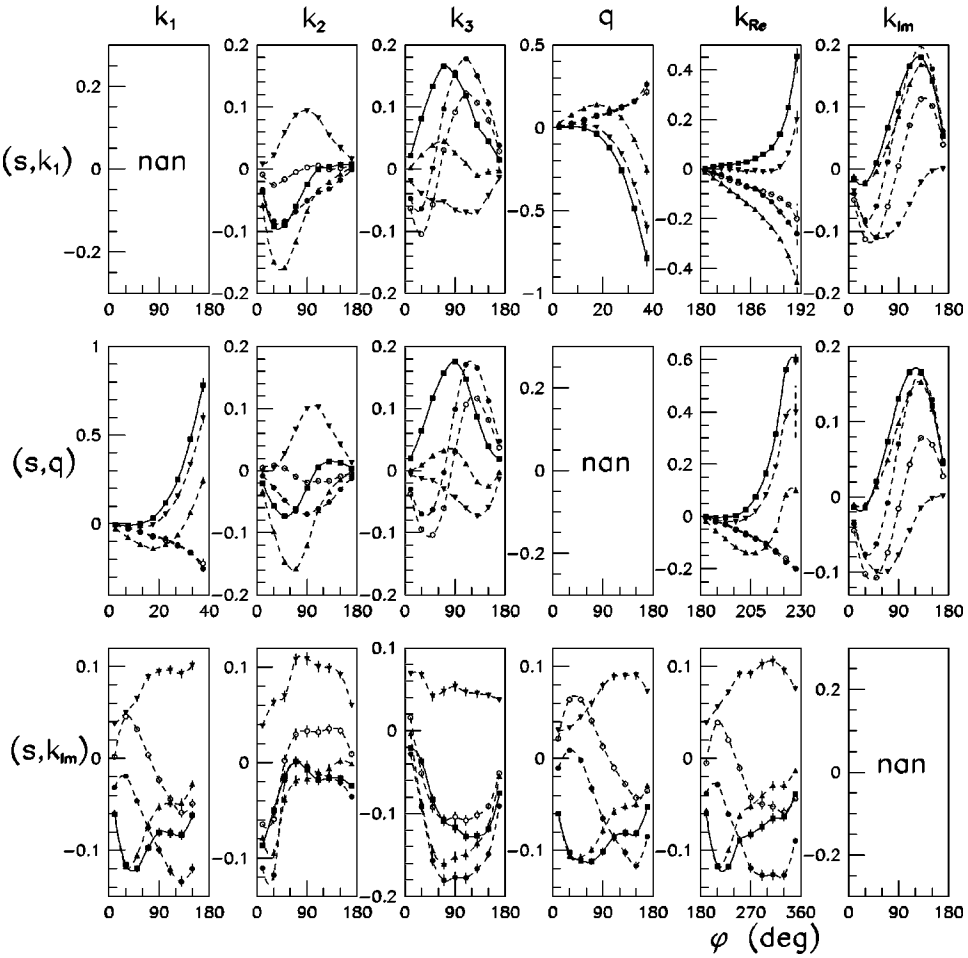

FIG. 5. Asymmetries for five solutions with the OPE parameters belonging to the ''ChPT'' set at ($\mathbf{s}\perp\mathbf{k}_1$) in the 4π-steradian geometry device; $\pi^- p^\uparrow\to\pi^-\pi^+ n$ reaction at $P_{\rm lab}=360$ MeV/c. The solid line marks the solution with best χ^2. The asymmetries for ($\mathbf{q},\mathbf{k}_1$) ($\mathbf{q},\mathbf{k}_{Im}$) ($\mathbf{k}_2,\mathbf{k}_3$) planes are near zero and not drawn.

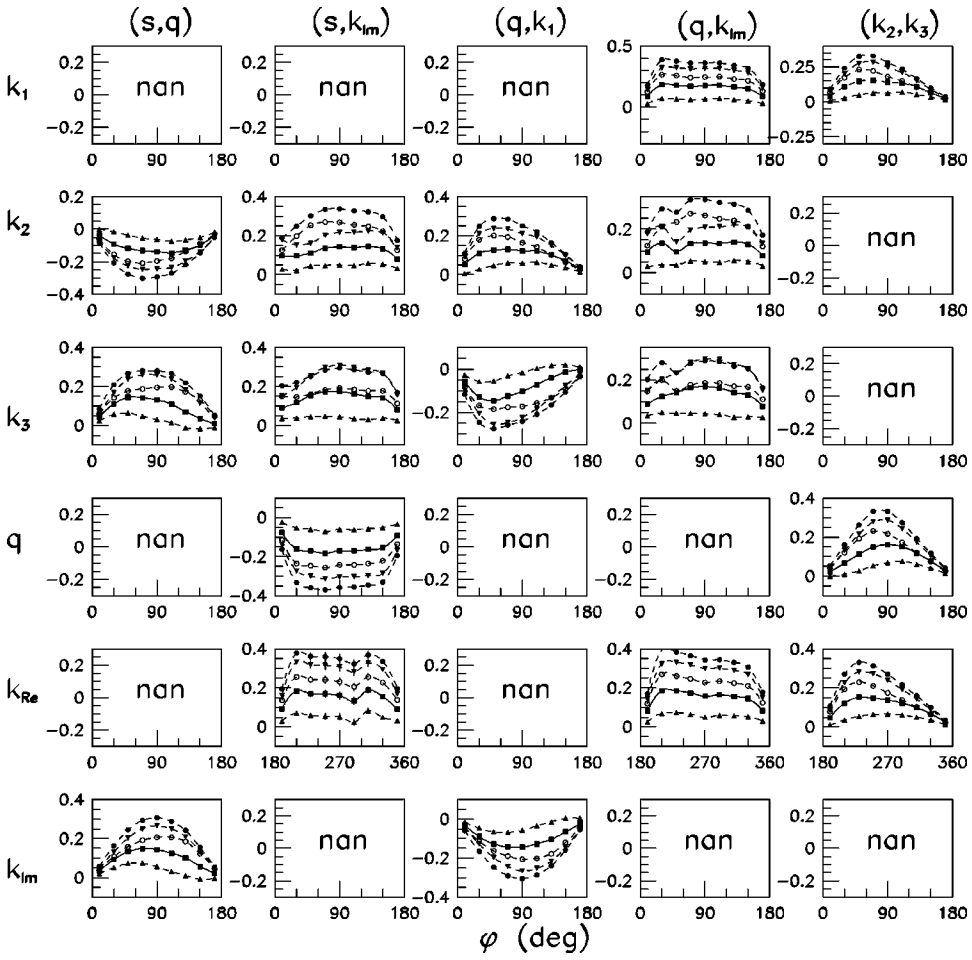

FIG. 6. Asymmetries for five solutions with the OPE parameters belonging to the ''ChPT'' set at $(\mathbf{s}||\mathbf{k}_1)$ in the 4π-steradian geometry device; $\pi^- p^\uparrow \to \pi^- \pi^+ n$ reaction at $P_{\rm lab}=360$ MeV/c. The solid line marks the solution with the best χ^2.

but one being found as solutions of an analysis [9] of unpolarized data, are used as theoretical input. These solutions are practically equivalent by the χ^2 criterion. Such properties of solutions like χ^2, errors of parameters, etc., are irrelevant for simulations. We show only specific values of $\pi\pi$-scattering lengths in Table I. The ordering of solutions in this table is performed according to the value of $a_0^{I=0}$. This reflects the role of OPE in the given amplitude: it is negligible for amplitudes at the bottom of Table I. The discussed amplitudes can be split into two classes: the *physical* amplitudes, which support the sequence of signs { ''+,'' ''−,'' ''+'' } for scattering lengths $a_0^{I=0}, a_0^{I=2}, a_1^{I=1}$, and the rest amplitudes, which we call *unphysical*. In Table I we display only *physical* amplitudes.

The amount of obtained data is too large to be displayed here. Table I collects the largest values of integral asymmetries found for the discussed amplitudes. Sometimes, a lower value is given if it is characterized by a better accuracy. The given errors are only statistical ones. This can help to estimate what number of experimental events is sufficient to detect the asymmetry in question.

In any case this table is not our guess about the possible values of $\pi\pi$-scattering lengths. On the contrary, it demonstrates that we cannot determine them without additional experimental data.

All data for asymmetries were also represented in graphical form. Only a few of them are shown in Figs. 1–8 for illustrative purpose. The figures are organized as a quasitable. Its columns correspond to various planes regarding to which asymmetry is measured. Two vectors, which determine this plane, are printed in brackets at the top of the column. The rows of these quasitables correspond to vectors, whose asymmetry as a little picture is shown in the cell as a small graph. For some elements of this quasitable the asymmetry does not exist because the vector row lies in the asymmetry plane. This case is marked by the abbreviation ''nan,'' which we borrow from UNIX and which means ''no a numbers.''

For example, a comparison of Fig. 1 with Fig. 2 helps to make conclusions on the role of the initial-spin orientation and on different properties of CHAOS selections.

The collection of figures is found to have a striking property: all solutions, being indistinguishable by χ^2 in the course of analysis [9], appear to be different.

Examination of the figures shows also that the asymmetries $A_{(\mathbf{s},\mathbf{q})}(\varphi_{\mathbf{k}_1})$, $A_{(\mathbf{s},\mathbf{q})}(\varphi_{\mathbf{k}_R})$, and $A_{(\mathbf{s},\mathbf{k}_1)}(\varphi_{\mathbf{q}})$ are characteristic of the OPE mechanism. These asymmetries become

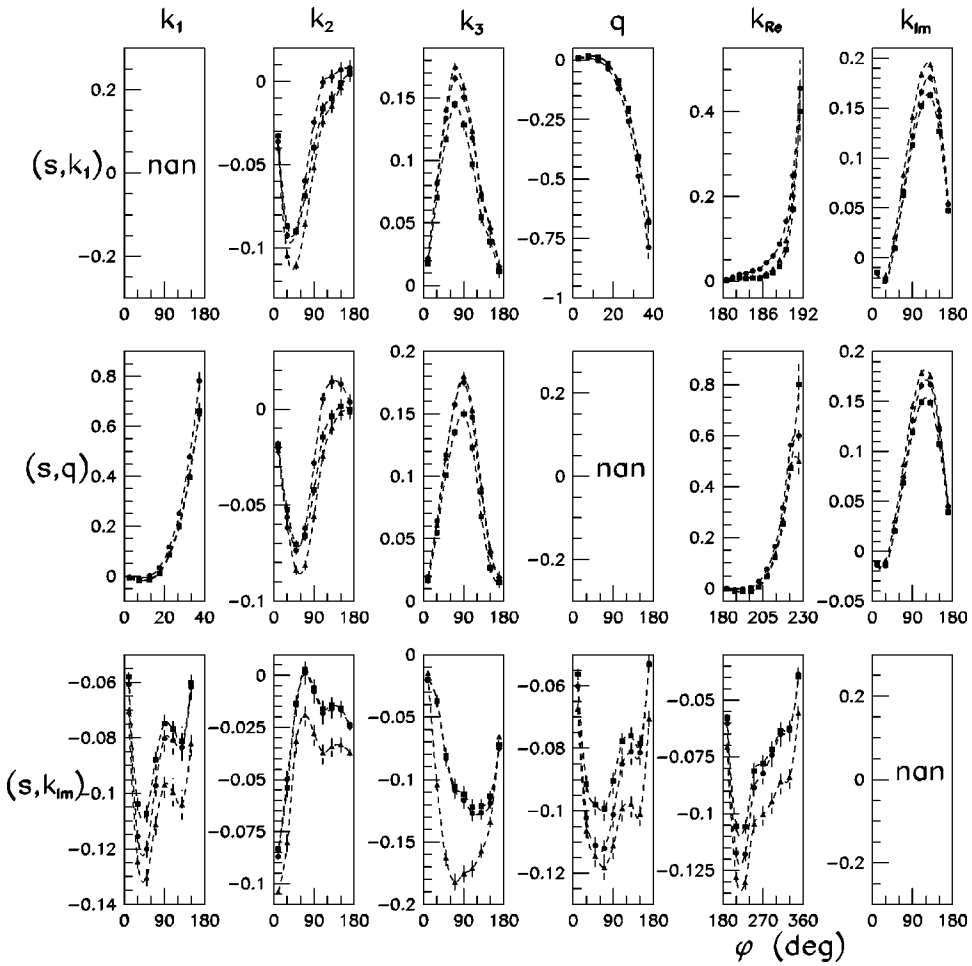

FIG. 7. Asymmetries for three solutions with the OPE parameters belonging to sets ''ChPT,'' ''GChPT,'' and ''Expt'' and best by χ^2 criteria within the each set at $(\mathbf{s}\perp\mathbf{k}_1)$ in the 4π–steradian geometry device; $\pi^- p^\uparrow \to \pi^-\pi^+ n$ reaction at $P_{\rm lab}=360$ MeV/c. The asymmetries for $(\mathbf{q},\mathbf{k}_1)$ $(\mathbf{q},\mathbf{k}_{Im})$ $(\mathbf{k}_2,\mathbf{k}_3)$ planes are near zero and not drawn.

smaller and other asymmetries start to appear when one is going from solutions at the top of Table I to solutions at the bottom, i.e., ''switching off'' the OPE contribution.

Another important feature of the obtained data is related to the unresolved ambiguity between the physical and unphysical solutions. It is found that the latter develop smaller asymmetries. Generally, the asymmetries for unphysical solutions are more difficult to detect, since they peak in the narrow angles characterized by low cross sections. In contrast, when asymmetries for physical amplitudes reach the maximal values, the curves are gently sloping. The absolute maximum $A\sim 1$ found corresponds usually to directions with small cross sections [see the distributions at $\varphi=40°$ given in Fig. 3; the corresponding asymmetry $A_{(\mathbf{s},\mathbf{q})}(\varphi_{\mathbf{k}_1})$ can be found in Fig. 1]. There are enough statistics for the nearby angles to detect the relatively high value of such asymmetry, for example, at $\varphi\sim 20°$; see Fig. 3.

When putting aside the last amplitudes from Table I and splitting the rest into physical and unphysical groups, a regular behavior of the figures with the parameter $a_0^{I=2}$ can be found in both groups. This is demonstrated by Fig. 4, where the asymmetries for physical amplitudes sol06, sol03, sol10, and solw6 are shown at $(\mathbf{s}\perp\mathbf{k}_1)$. The almost smooth transformation of one picture into another is clearly seen for asymmetries, which are relevant to OPE. This regularity and the absence of the same regularity for $a_0^{I=0}$ variation can be interpreted as indirect evidence in favor of smaller perturbations by isobar contributions to the isospin $I=2$ amplitude. However, poor asymmetries from OPE and the rich rest ones obtained for the $\pi^+ p^\uparrow \to \pi^+\pi^+ n$ channel do not support this.

These conclusions are valid for measurements with $(\mathbf{s}\perp\mathbf{k}_1)$ in devices with 4π-steradian geometry and in the CHAOS device as well. Moreover, the CHAOS geometry selects events displaying larger asymmetries, though at the price of lower statistics.

The asymmetries for the setup $(\mathbf{s}||\mathbf{k}_1)$ are rich and informative for the 4π-steradian geometry of a hypothetical device. Here, the asymmetries $A_{(\mathbf{q},\mathbf{k}_1)}(\varphi_{\mathbf{z}})$, $A_{(\mathbf{q},\mathbf{k}_I)}(\varphi_{\mathbf{z}})$, and $A_{(\mathbf{k}_2,\mathbf{k}_3)}(\varphi_{\mathbf{z}})$ $(\mathbf{z}=\mathbf{k}_1,\mathbf{k}_2,\mathbf{k}_3,\mathbf{k}_R,\mathbf{k}_I,\mathbf{q})$, all of which are almost flat for a $(\mathbf{s}\perp\mathbf{k}_1)$ setup, look much more vivid (cf. Figs. 1 and 2). According to the criteria of Sec. III, the ''switching off'' effect of $(\mathbf{s}\cdot\mathbf{k}_R)\sim -(\mathbf{s}\cdot\mathbf{k}_1)=0$ must be solely due to non-OPE mechanisms in the test amplitudes. These are indeed present in all discussed solutions.

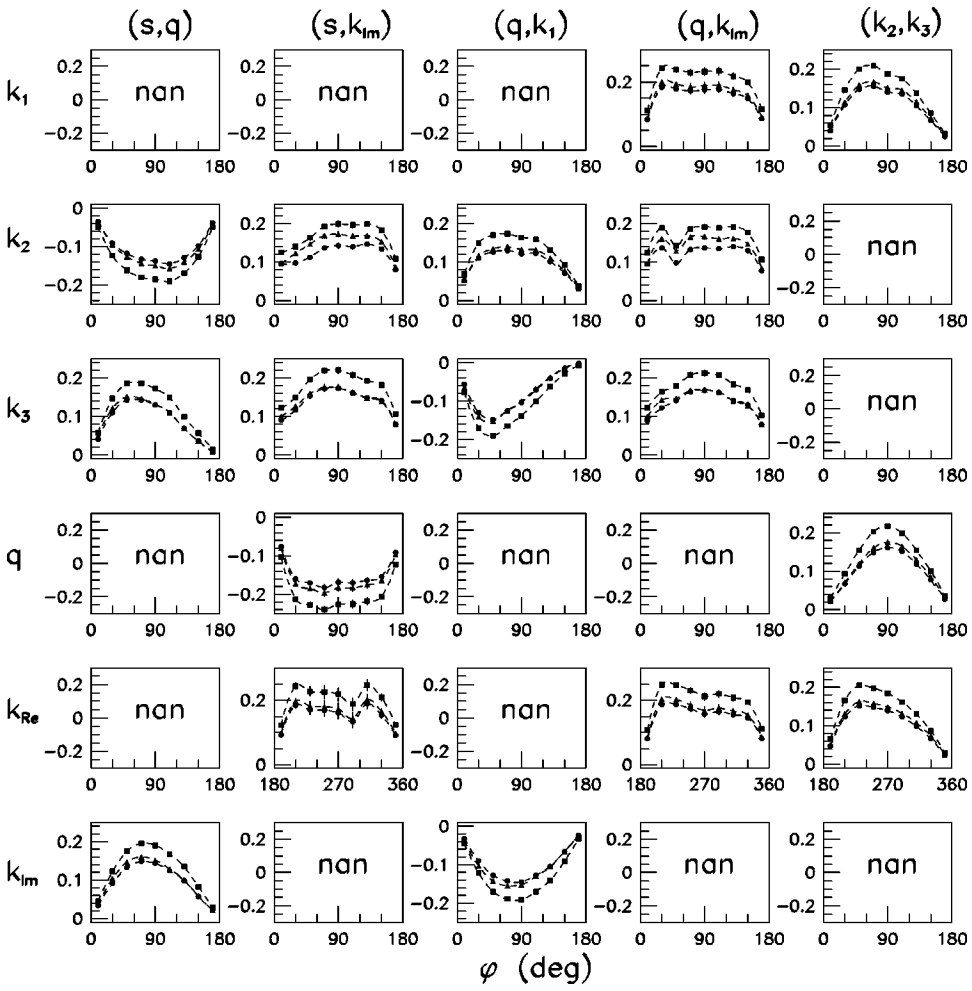

FIG. 8. Asymmetries for three solutions with the OPE parameters belonging to sets ''ChPT,'' ''GChPT,'' and ''Expt'' and best by χ^2 criteria within each set at $(\mathbf{s}||\mathbf{k}_1)$ in the 4π-steradian geometry device; $\pi^- p^\uparrow \to \pi^- \pi^+ n$ reaction at $P_{\rm lab}=360$ MeV/c.

When projected to CHAOS, all examined asymmetries for $(\mathbf{s}||\mathbf{k}_1)$ appear to be consistent with zero. This is not so surprising, since, for the $(\mathbf{s}||\mathbf{k}_1)$ setup, practically all interesting events happen in the plane which is orthogonal to the beam $\mathbf{k}_1$. Most such events avoid CHAOS chambers. Though the cross sections themselves are found to be sensitive to the tested amplitudes in the forward and backward cones, it is difficult to evaluate the importance of such data. One can recall that the above critical plane is entirely accepted by the wire-chamber space of the design for the AMPIR spectrometer [23]. This remarkable complementarity of CHAOS and AMPIR devices makes a promise for exhaustive investigations of polarization effects in $\pi N \to \pi\pi N$ reactions at low energies.

The selection of solutions which have $\pi\pi$-scattering lengths close to the values usually accepted cannot resolve the ambiguity problem. To check this we have made a fit of the experimental data without polarization observables with an amplitude which had the $\pi\pi$-scattering lengths fixed by the values taken from the modern literature. We used three sets of such values taken from [28]. We present these values in Table II. For each set we made 100 random starts. For each set we have obtained five different solutions. For each set we calculated asymmetries. Figures 5 and 6 show the asymmetry for $\pi\pi$ parameters from the set ''ChPT.'' It is seen that various solutions generate quite different asymmetry pictures. So the criterion of ''reasonableness'' of $\pi\pi$ parameters is not sufficient to make a decision whether the solution is good or bad.

Figures 7 and 8 demonstrate the asymmetries for three amplitudes, each of which is the best by χ^2 criteria within each $\pi\pi$ set. The difference between the asymmetries, generated by these three amplitudes, is very small, so it is difficult to hope that asymmetry measurements will help us to make a choice between ChPT and GChPT theories.

We finish the discussion of results by recalling that there are simplifications in the procedure. The incomplete polarization in the real experiment can decrease the absolute values of the shown asymmetries by a few percent. The real-device efficiency and the reduced experimental statistics enlarge errors. The number of generated events in simulations ($\sim 4\times 10^4$ hitting CHAOS) represents the lowest limit ever attainable experimentally. Provided no confident result is obtained, the problem of polarization phenomena below the isobar threshold $P_{\rm lab}<500$ MeV/c would be closed. The rich picture of effects displayed by almost every amplitude at

$P_{\rm lab}=360$ MeV/c is far above cautious expectations. The magnitude of statistical errors given in Table I demonstrates that the number of experimental events which is necessary to detect the discussed phenomena and discriminate between competing contributions can be decreased by an order of magnitude. It must be noted that the reaction channel $\pi^- p^\uparrow \to \pi^- \pi^+ n$ is not the best one with respect to the integral asymmetries examined in this section. Simulations with some selected amplitudes show the following order of preference: $\pi^+ p^\uparrow \to \pi^+ \pi^0 p$, $\pi^- p^\uparrow \to \pi^- \pi^0 p$, $\pi^- p^\uparrow \to \pi^- \pi^+ n$, $\pi^+ p^\uparrow \to \pi^+ \pi^+ n$, $\pi^- p^\uparrow \to \pi^0 \pi^0 n$. This means that the neutral channel requires full-kinematics measurements for detecting asymmetries in distinct regions of the entire phase space.

V. CONCLUSIONS

The main achievement of the present paper is the demonstration of the striking efficiency of the polarization measurements for $\pi N \to \pi\pi N$ reactions in the energy region very close to threshold. Such measurements are feasible with the use of the CHAOS spectrometer right now. This is shown in the framework of the standard formalism adjusted to the canonical form of the $\pi N \to \pi\pi N$ amplitude [20,22].

The motivation for such experiments follows from the disappointing difficulties encountered within the frameworks of all known methods for an analysis of low-energy $\pi N \to \pi\pi N$ data. The deep reason for the difficulties in the interpretation of the $\pi N \to \pi\pi N$ results is related to the very nature of the unpolarized data which cannot help in discriminating between the t-channel mechanism of OPE and isobar exchanges.

The competition between OPE and the rest mechanisms of the $\pi N \to \pi\pi N$ reaction, preventing an accurate determination of the $\pi\pi$ interaction with the help of unpolarized data, at the same time gives rise to extremely rich polarization effects within the half-width isobar region.

The effects are found to be sensitive to the OPE parameters in question as well as to details of isobar interactions. All equivalent solutions of Ref. [9] appear to be different in the asymmetry picture. Therefore, any project of the determination of the parameters of the $\pi\pi$ interaction with the help of $\pi N \to \pi\pi N$ data must assume the polarization measurements. The yield for a decisive $\pi N \to \pi\pi N$ analysis must combine both unpolarized data and polarization information.

Application of the results of the present paper is straightforward within our approach. It is simple to find that all asymmetries vanish in the extrapolation points specific to Chew-Low methods. This can help to estimate a part of the theoretical error characteristic of the method. Indeed, provided the data of polarized-target experiments are collected separately from right and left semispheres with respect to $(\mathbf{s},\mathbf{k}_1)$, $(\mathbf{s},\mathbf{q})$, or $(\mathbf{q},\mathbf{k}_1)$ planes, an estimate of the error is obtained by independent extrapolations.

ACKNOWLEDGMENTS

A.A.B. and S.G.S. thank the Russian Foundation for Basic Research for support in terms of Grant No. 95-02-05574a. We are grateful to G.A. Feofilov and D. Počanić for remarks and to members of the CHAOS Collaboration, P. Amaudruz, F. Bonutti, J. Brack, P. Camerini, E. Fragiacomo, N. Grion, G. Hofman, R.R. Johnson, S. McFarland, M. Kermani, R. Rui, M. Sevior, G.R. Smith, and R. Tacik, for various help and discussions.

[1] J. Gasser and H. Leutwyler, Phys. Lett. **125B**, 312 (1982); **125B**, 325 (1982).
[2] J. Gasser and H. Leutwyler, Ann. Phys. (N.Y.) **158**, 142 (1984); Nucl. Phys. **B250**, 465 (1985); **B250**, 517 (1985); **B250**, 539 (1985).
[3] S. Weinberg, Phys. Rev. Lett. **17**, 616 (1966).
[4] S. Weinberg, Phys. Rev. **166**, 1568 (1968).
[5] S. Weinberg, Physica A **96**, 327 (1979).
[6] J. Stern, H. Sazdjian, and N. H. Fuchs, Phys. Rev. D **47**, 3814 (1993).
[7] D. Počanić, in *Chiral Dynamics: Theory and Experiment*, Proceedings of the Workshop held at MIT, Cambridge, MA, 1994, edited by A. M. Bernstein and B. R. Holstein, Lecture Notes in Physics, LNP 452 (Springer-Verlag, Berlin, 1995), p. 95.
[8] D. Počanić, ''Low Energy Experiments on π-π Scattering,'' Report No. UVA-INPP-98-01, 1997; ''Talk given at Workshop on Chiral Dynamics: Theory and Experiment (ChPT 97),'' Mainz, Germany, 1997, hep-ph/9801366.
[9] A. A. Bolokhov, M. V. Polyakov, and S. G. Sherman, Eur. Phys. J. A **1**, 317 (1998).
[10] D. Počanić and E. Frlež, Nucl. Phys. **A629**, 201c (1998).
[11] M. G. Olsson, Phys. Lett. B **410**, 311 (1997).
[12] O. O. Patarakin, ''A Measurement of the $\pi^\pm p \to \pi^+ \pi^\pm n$ Reactions Near Threshold,'' in Ulf–G. Meissner *et al.* ''Working Group on $\pi\pi$ and πN Interactions. Summary,'' Report No. KFA-IKP-TH-1997-21, 1997; ''Summary of the working group on $\pi\pi$ and πN interactions given at Workshop on Chiral Dynamics: Theory and Experiment (ChPT 97),'' Mainz, Germany, 1997, hep-ph/9711361.
[13] M. E. Sevior, ''Determination of the $\pi^\pm p \to \pi^\pm \pi^+ n$ Cross-Sections Near Threshold,'' in Ulf–G. Meissner *et al.*, ''Working Group on $\pi\pi$ and πN Interactions. Summary,'' Report No. KFA-IKP-TH-1997-21, 1997; ''Summary of the working group on $\pi\pi$ and πN interactions given at Workshop on Chiral Dynamics: Theory and Experiment (ChPT 97),'' Mainz, Germany, 1997, hep-ph/9711361.
[14] D. M. Manley, Phys. Rev. D **30**, 536 (1984).
[15] A. de Lesquen *et al.*, Phys. Rev. D **32**, 21 (1985).
[16] G. Grayer *et al.*, Nucl. Phys. **B75**, 189 (1974).
[17] M. Svec, Phys. Rev. D **46**, 949 (1992).
[18] H. Becker *et al.*, Nucl. Phys. **B151**, 46 (1979).
[19] G. R. Smith *et al.*, Nucl. Instrum. Methods Phys. Res. A **362**, 349 (1995).

[20] A. A. Bolokhov, V. V. Vereshchagin, and S. G. Sherman, Yad. Fiz., **47**, 491 (1988) [Sov. J. Nucl. Phys. **47**, 311 (1988)].
[21] A. A. Bolokhov, V. V. Vereshchagin, and M. V. Polyakov, Yad. Fiz., **48**, 811 (1988) [Sov. J. Nucl. Phys. **48**, 517 (1988)].
[22] A. A. Bolokhov, V. V. Vereshagin, and S. G. Sherman, Nucl. Phys. **A350**, 660 (1991).
[23] A. B. Kurepin *et al.*, ''Spectrometer AMPIR for Investigation of Rare and Multiparticle Processes,'' Institute for Nuclear Research, Russian Academy of Sciences, Report No. INR-769/92, Moscow, 1992.
[24] V. V. Anisovich and A. A. Anselm, Sov. Phys. Usp. **88**, 287 (1966).
[25] A. C. Hern, REDUCE User's Manual, Rand Corp., Santa Monica, 1985.
[26] F. Bonutti *et al.*, Nucl. Instrum. Methods Phys. Res. A **337**, 165 (1993).
[27] F. Bonutti *et al.*, Nucl. Instrum. Methods Phys. Res. A **350**, 136 (1994).
[28] J. Bijnens *et al.*, Nucl. Phys. **B508**, 263 (1997).